Application of high-resolution remote sensing to landform evolution in Central Nepal following the 2015 Gorkha earthquakes

Lauren Hutchinson
Department of Earth Sciences – Simon Fraser University, Burnaby, British Columbia, Canada
BGC Engineering Inc., Vancouver, British Columbia, Canada
Doug Stead
Department of Earth Sciences – Simon Fraser University, Burnaby, British Columbia, Canada
Nick Rosser
Institute of Hazard, Risk and Resilience – Durham University, Durham, United Kingdom

ABSTRACT
This paper presents the results of a 5-year investigation of two case study slopes in Central Nepal using data from a range of remote sensing techniques used both prior to and following the 2015 M_w Gorkha earthquake. A primary focus of this work is change detection at a rock slope using high resolution, full waveform terrestrial laser scans collected in 2012, three years prior to the 2015 earthquakes with scans collected following the annual South-Asian monsoon cycles in 2016 and 2017. Our findings indicate strong structural control on pre-earthquake instability and a concentration of failures at locations where instability pre-dated the earthquakes. We also find that post-seismic failures predominantly involve movement of colluvium downslope through debris flows during monsoonal rainfall from the existing co-seismic landslides with to date limited observed failure from new source areas. The application of ground-based remote sensing techniques to characterize landform evolution in remote high mountainous areas is demonstrated and future research directions discussed.

RESUME
Cet article présente les résultats d'une étude de deux pentes au Népal Centrale pendant cinq ans à l'aide d'une gamme de techniques de télédétection couvrant la période avant et après le séisme de Gorkha (M_w 7.8) en 2015. L'objectif principal de cette étude est la détection de changements sur une pente rocheuse en utilisant les données de balayage laser terrestre à haute résolution acquis en 2012, trois ans avant les séismes de 2015, avec ceux acquis suivant les cycles annuels de mousson sud-asiatique en 2016 et 2017. Les résultats indiquent un fort contrôle structural de l'instabilité pré-sismique et une concentration d'éboulements aux endroits où l'instabilité est antérieure aux séismes. Nous constatons également que les glissements de terrain post-sismiques impliquent principalement le transport des matériaux colluvions par des coulées de débris pendant les pluies de mousson à partir des ruptures co-sismiques existantes avec, jusqu'à présent, peu de glissements observés en provenance de nouvelles sources. L'application de techniques de télédétection terrestre pour caractériser l'évolution du terrain dans les régions montagneuses éloignées est démontré et les directions de recherche futures discutées.

1 INTRODUCTION

Assessment of the post-seismic response of slopes is a critical component of response and recovery work following large earthquakes. Researchers have long focused on the distribution and spatial extent of earthquake-triggered landslides (Keefer 1984, 2000, 2002, Rodríguez et al. 1999, Jibson et al. 2000, Bommer and Rodríguez 2002, Jibson 2011). Mapping efforts following large earthquakes in Taiwan (Tatard and Grasso 2013, Lin et al. 2016), India (Barnard et al. 2001), Pakistan (Owen et al. 2008), and China (Gorum et al. 2011, Yang et al. 2017) have shown the extent of landsliding that occurs in response to these events.

Recently, researchers have focused on the legacy of earthquakes on a given landscape and in particular the phenomena of reduced thresholds for post-seismic landslide triggering by rainfall and future seismicity (Moore et al. 2012, Marc et al. 2015, Parker et al. 2015). These studies have illustrated a longer-term impact of seismicity on the surrounding landscape wherein the seismic events make the slope more susceptible to future failure.

The process of repeated, cyclic loading of the slope from gravitational, hydrological and seismic stresses resulting in progressive accumulation of damage in brittle slope materials is suggested to ultimately lead to the overall increased susceptibility to failure (Moore et al. 2012, Parker et al. 2015, Gischig et al. 2015). At present, detailed field-based assessment of seismically-induced damage accumulation is limited by a lack of high-resolution monitoring data to allow detailed comparison of the pre- and post-earthquake conditions of a slope and better understand the slope failure mechanisms.

The 2015 earthquake sequence in Nepal triggered over 25,000 landslides covering a mapped area of 87 km^2 (Roback et al. 2016). The distribution of landslides is

concentrated between the epicentres of the mainshock and the two main aftershocks in Central Nepal. High landslide densities have been observed in areas with steep slopes, high annual precipitation and proximity to fault rupture. The highest densities exist in areas where these characteristics overlap with one another (Roback et al. 2016).

To date, the majority of research on the Gorkha earthquakes and associated landsliding has focused on rapid assessment (Collins and Jibson 2015, Robinson et al. 2017, Williams et al. 2017) and remote mapping of landslides (Kargel et al. 2016, Martha et al. 2016, Roback et al. 2016, Tiwari et al. 2017). In order to better understand the mechanisms of slope response, in particular in the monsoonal climate of Nepal, detailed slope-scale studies are required.

2 STUDY AREA

The Upper Bhote Koshi (UBK) river valley is located in Sindhupalchok District, Central Nepal (Figure 1). The valley straddles the boundary of the Lesser and Higher Himalayan geological zones which are separated by the Main Central Thrust (MCT) fault near the northern border of Nepal with Tibet. The Higher Himalayan sequence is comprised primarily of Proterozoic augen and banded gneisses and forms the hanging wall of the MCT to the north. The Lesser Himalaya is characterized by folds and faults developed when the Higher Himalaya crystalline thrust sheet overrode the Lesser Himalaya Sequence (Dhital 2015).

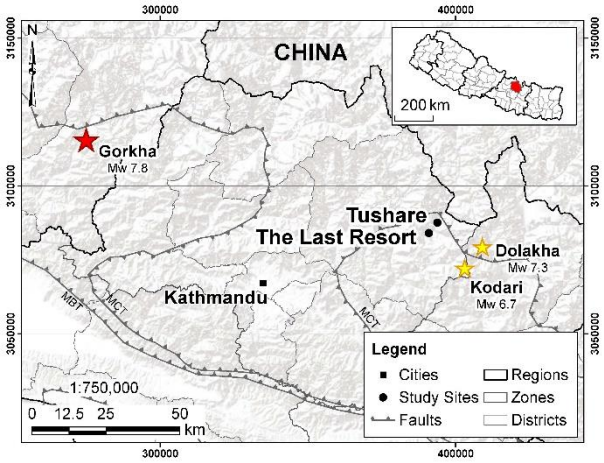

Figure 1. Map of study area showing the locations of the 2015 mainshock (red) and principal aftershocks (yellow). Inset shows Sindhupalchok district in red. Base topographic map source ESRI, USGS, NOAA (ESRI 2017). Coordinates are WGS 1984 UTM Zone 45N.

Due to the proximity to the MCT, Sindhupalchok along with the neighbouring districts forms an area of seismic clustering evident on epicentral maps (National Seismological Centre (NSC) 2016). Hundreds of earthquakes with local magnitudes (ML) less than 4 are recorded on a monthly basis in Nepal, northern India and southern Tibet with a further 5 to 20 ML 4-5 earthquakes monthly (Figure 2). The records available are incomplete but provide a good indication of the level of seismic activity along with the general decay with time since the 2015 earthquake sequence.

The known association between seismic loading and damage accumulation in rock slopes (Stead and Eberhardt 2013, Gischig et al. 2015, Wolter et al. 2015) suggests that the seismic loading from lower magnitude earthquakes may play a significant role in governing the stability of slopes over time in the UBK.

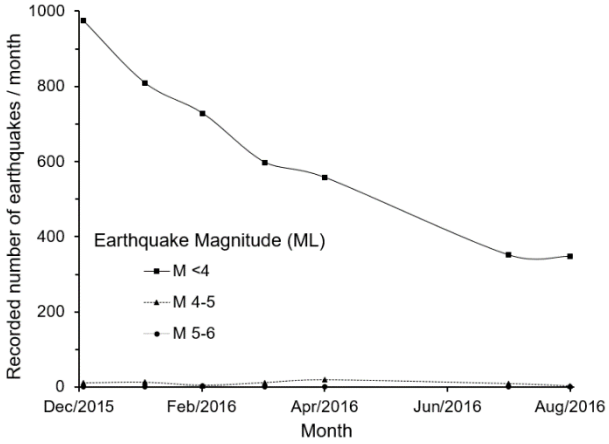

Figure 2. Number of earthquakes recorded by the NSC between December 2015 and August 2016 across Nepal, northern India and southern Tibet. In the time period presented, no earthquakes with magnitudes (ML) exceeding 6 were recorded.

The UBK valley slopes range from approximately 25° to near vertical walls along sections of the Araniko Highway that runs adjacent to the Bhote Koshi river and connects the capital of Nepal, Kathmandu to the Tibetan border. Elevation in the valley ranges from approximately 1200 metres above sea level (masl) along the Bhote Koshi to 3400 masl on the eastern valley ridge tops (ASTEM GDEM).

Annual precipitation in the UBK ranges from 2500 mm to >4000 mm due to the strong orographic effects of the high mountains to the north in Tibet with approximately 71-92% of the precipitation occurring during the monsoon cycle between June and September (Adhikari & Koshimizu, 2005; Petley et al., 2007). The annual monsoonal cycle has a strong control on landslide activity across Nepal (Petley et al. 2007) which is consistent with observations of landsliding in the UBK as discussed by Oven (2009).

We investigated two slopes, Tushare and The Last Resort, in the UBK (Figure 1) and compare and contrast the behaviour in response to the 2015 earthquakes and subsequent annual monsoon cycles in 2016 and 2017.

3 METHODS

We mapped the aerial extent of co- and post-seismic landslides at Tushare and TLR on satellite imagery from September 2015 at resolution of 0.5 m (Pleiades 2015). Cloud cover associated with the annual monsoon between June and September limited the quality of satellite imagery

prior to this date. The mapped extent of landsliding at each site was 0.4 km^2 along the ridge surrounding Tushare and 0.03 km^2 at TLR, including the failures denoted a-d in Figure *5*, Figure 6.

We collected terrestrial laser scans (TLS) and high resolution terrestrial digital photography (TDP) following the 2016 and 2017 monsoon cycles at both slopes (Table 1). TLS data covers the full slope with average point spacing of between 0.07 m and 0.2 m. Select windows were scanned at higher resolution with mean point spacing of 0.02 m to 0.07 m. At Tushare, these data are supplemented with pre-earthquake TLS data collected in 2012 by Durham University (mean point spacing 0.18 m to 0.70 m).

We collected aerial imagery in November 2016 using a system of GoPro cameras mounted to the skids of a helicopter to collect near constant footage over the UBK supplemented with handheld digital photography collected during the overflight. At both sites, these data are supplemented with video footage collected by the United States Geological Survey (USGS) during the rapid assessment completed following the earthquakes (Collins and Jibson 2015).

Table 1. Data collection methods

Method	Sept 2012	May 2015	Sept 2015	Nov 2016 / Oct 2017
TLS	Riegl VZ-1000		-	Riegl VZ-4000
TDP	-		-	Canon EOS 5DS [1] Gigapan robotic head
Satellite	-		PLEIADES (0.5 m)	-
Aerial Imagery	-	USGS [2]		GoPro [3]

[1] 50 MP, *ƒ* 50 mm, 200 mm, 400 mm
[2] May 27, 2015 helicopter overflight by (Collins 2015)
[3] 4 cameras, image capture every 0.5 seconds.

TLS data were aligned and registered in RiSCAN Pro (RIEGL 2016). Vegetation was removed by extracting non-ground returns and applying filters to remove points outside specified deviation and reflectance ranges before applying the RiSCAN Pro vegetation filter and manually editing as required. The bare earth clouds were imported to CloudCompare (Girardeau-Montaut 2017) for analysis and rasterization. Slope-scale rasters (0.5 m resolution) were imported to ArcGIS (ESRI 2017) for engineering geomorphological mapping (Griffiths and Whitworth 2012) and two-dimensional change detection. We considered change greater than the raster pixel size (0.5 m) resolution only where point densities in both rasters exceeded 4 pts/cell as determined by the number of neighbours calculated per cell in CloudCompare. A mask was applied to exclude all surface change measurements where the slope angle exceeds 60° given the limitation of this process to near-vertical slopes (Lague et al. 2013).

Change detection results were compared with results for the same datasets using the M3C2 plugin (Lague et al. 2013) in CloudCompare to ensure fidelity between the two and three-dimensional techniques.

Evaluation of earthquake and monsoon impacts at the outcrop scale using a comparative assessment of TLS and high-resolution TDP where the resolution and/or occlusion of the TLS data does not provide a sufficient level of detail to discern changes is a focus of ongoing work.

Video stills were extracted from the USGS footage using ffmpeg (FFmpeg 2016) and developed into Structure from Motion (SfM) models using PhotoScan (Agisoft LLC. 2014). The imagery collected in the 2016 helicopter overflight was also processed in PhotoScan. These models were georeferenced and aligned to the TLS data in CloudCompare (Girardeau-Montaut 2017). The SfM models served to fill occluded areas in the TLS data and in the case of the 2015 model, added an additional epoch to help delineate which movements occurred prior to the 2015 monsoon as compared with those that were monsoon rainfall-triggered.

To complement slope scale change detection, we developed engineering geomorphological maps using the ground-based TLS data to map morphometric slope changes, delineate mass movements and headscarps in ArcGIS (ESRI 2017) at 1:5000 scale in order to better understand geomorphological constraints on slope behaviour.

4 OBSERVATIONS

4.1 Tushare

Tushare (Figure *3*) is located on the west side of the Araniko Highway and Bhote Koshi river approximately 4.5 km south of the border with Tibet. It is within 25 km of the epicentres of the two main aftershocks (Figure 1). The slope is approximately 560 m in height ranging from 1250 masl to 1810 masl with an average slope angle of approximately 42°. At midslope, an approximately 70 m high subvertical rockface is observed.

Figure 3.Tushare landslide (October 5, 2017).

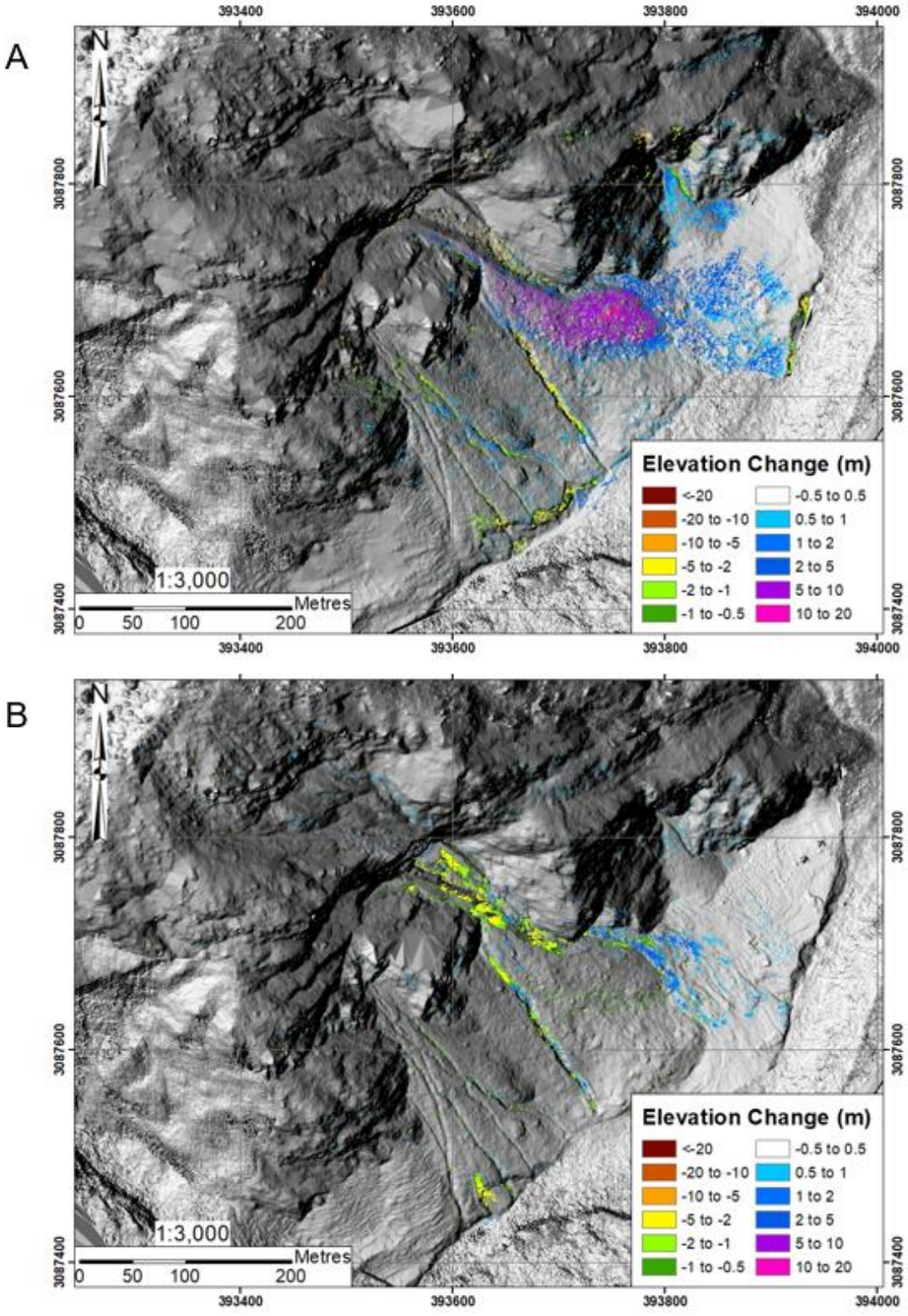

Figure 4.Plots showing elevation change at Tushare. Warm colours show erosion and cool colours show deposition. A) Change between September 20, 2012 and November 6, 2016 shown on 0.5 m TLS DEM from November 6, 2016. B) Change between November 6, 2016 and October 5, 2017 shown on 0.5 m TLS DEM from 2017. In both, the background DEM is based on SfM model from helicopter overflight on November 8, 2016.

The change detection results (Figure 4) reveal insights to the failure modes affecting the slope during and following the earthquakes.

4.1.1 September 2012 to November 2016

Figure 4A shows change between September 20, 2012 and November 6, 2016. As evident in Figure *3*, the slope at Tushare is governed by three dominant, highly persistent (>20 m) discontinuity sets (ISRM 1978). Outcrops of bedrock following these discontinuity surfaces control where material was eroded and subsequently deposited during the earthquake triggered landslides.

The relatively low point density of the upper slope in the 2012 scans (<4 pts/cell) due to a combination of the range of the scanner, occlusion due to scanning angle and the focus of the scans on the lower slopes does not allow identification of the failure mode and volume above the rockface from the change detection results alone. Instead, aerial imagery provides a better indication of the characteristics of the upper slope which constitutes the main source area of the landslide.

The main deposit is characteristic of a flow-type failure and given the timing of the earthquakes (pre-monsoon) this would likely be a predominantly dry, frictional flow.

Incision of the landslide debris evident on the east side of the deposit indicates movement with higher fluid content based on the flow lines in the deposited material. For this reason, we hypothesize that the incision occurred post-earthquake in a series of events during the 2015 and 2016 monsoon seasons that pre-dated the 2016 scans.

Channel incision into the vegetated, debris apron at the base of the slope is also evident. To the east of the main failure, a rockfall that pre-dated the 2012 data collection shows evidence of reactivation of the source area and incision of the talus cone.

Channel bank erosion at the base of the slope associated with a July 2016 glacial lake outburst flood (Cook et al. 2017) is evident up (right) and downstream (left) of the main failure.

Limitations to the results include the lower point density in the upper slope above the rock face in the 2012 scans, as discussed, as well as inaccuracies associated with the line of sight for the 2D change detection. Subvertical sections of the slope are oriented perpendicular to the change detection line of sight along the Z-axis making material loss from these faces undetectable. For this reason, two rockfalls on the east and west sides of the main rock face at midslope (Figure 3) that contributed significant volumes of material are not shown.

4.1.2 November 2016 to October 2017

Figure 4B shows change between November 6, 2016 and October 5, 2017 and indicate movements up to 5 m incision/deposition on the slope during the 2017 monsoon. Further incision into the earthquake-triggered landslide debris and remobilization of material in debris flow(s) is evident. Additionally, channel incision in the debris apron in the lower third of the slope continued in the 2017 monsoon. The depth of incision is greatest in the channel immediately west of the debris where the channel is 5 to 10 m wide and incised up to 4.5 m in the 2017 monsoon. The TLS data in concert with photography from 2017 (Figure *3*) suggest that an avulsion may be developing at the apex of the landslide debris and could continue in subsequent monsoon seasons.

4.2 The Last Resort (TLR)

TLR (Figure *5*) is located on the north side of the Araniko Highway and Bhote Koshi river approximately 9 km south of the border with Tibet. As with Tushare, it is within 25 km of the epicentres of the two main aftershocks of the 2015 earthquakes (Figure 1). TLR is located at an elevation of approximately 1200 masl and is on the lower half of a slope which extends from the Bhote Koshi River, in the canyon below TLR, up to approximately 1950 masl.

The slope above TLR experienced several mass movements during the 2015 earthquake sequence including reactivation of pre-existing failures visible on pre-earthquake satellite imagery.

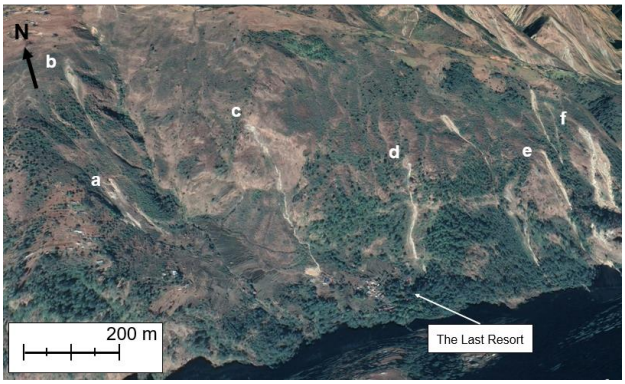

Figure 5.Slopes above The Last Resort from Google Earth imagery dated December 8, 2017. The letters correspond to the features shown on Figure 6.

A similar change detection procedure was applied at TLR as used at Tushare, however, no significant changes exceeding the 1.0 m slope-scale level of detection were observed. Outcrop scale change detection including a comparative analysis of high-resolution TDP and TLS is part of ongoing work.

In order to better understand the evolution and constraints on mass movements on the slopes above TLR, engineering geomorphological maps were developed based on the TLS imagery (Figure 6). The slopes above TLR exhibit a range of range of failure processes including landslides (a, c), debris slide - debris flows (b, e-f), and rockfall (d).

Alignment of lineaments on the slope with instabilities both from before and after the earthquakes (Figure 6B) illustrates a strong structural control on the locations of slope failures.

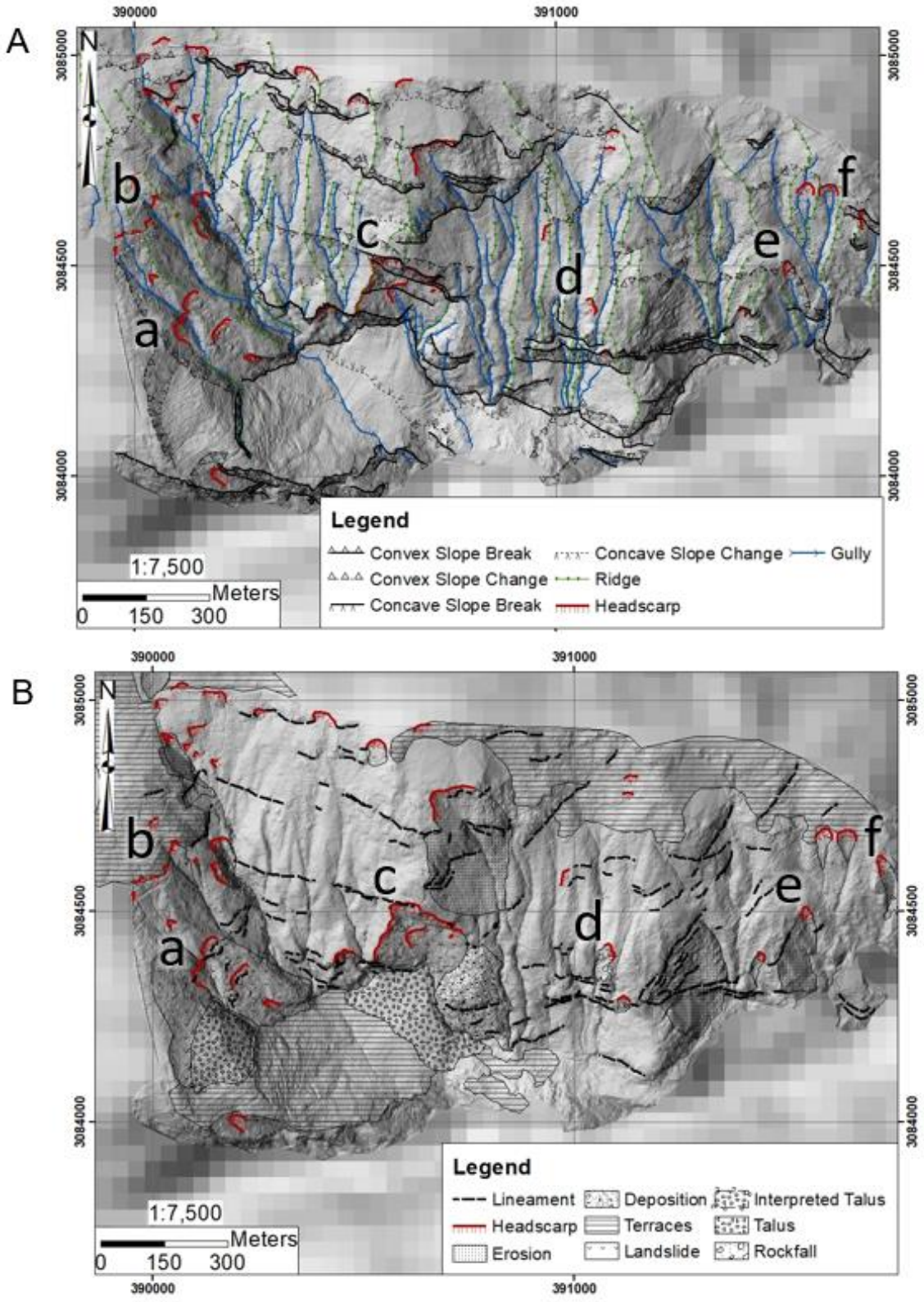

Figure 6.Engineering geomorphological maps based on November 6-7, 2016 and October 6, 2017 TLS data. Basemap underlying TLS is 1-arcsecond ASTER gDEM. A) Morphometric map of slope change, B) Map of mass movements and lineaments. The letters correspond to the same features in Figure 5.

5 DISCUSSION

The two slopes investigated provide examples of slope behaviour characteristic of the post-earthquake landscape of the UBK. At Tushare, the annual monsoon cycle in 2015, 2016 and 2017 has continued to remobilize debris from the existing deposits through episodic debris flows and sediment transport by channel incision. Based on the evidence from late 2017, we expect this behaviour to persist in the 2018 monsoon. There is limited evidence of new signs of instability at Tushare indicating that the post-seismic slope instability is concentrated in areas that exhibited failures prior to the earthquakes or were triggered during the earthquakes.

In contrast, at TLR, the post-seismic changes to the slope are less noticeable and often require that TLS data be supplemented with high-resolution TDP to discern movement. The failures show a strong structural control with headscarps occurring where linear features intersect one another or at marked changes in the slope profile.

At both slopes, loose rock and debris exist in the upper slopes and are expected to remobilize in the future. Ongoing monitoring of the slopes following each monsoon will provide greater insight into the medium-term response of earthquake affected slopes to the annual monsoon.

6 CONCLUSIONS

This preliminary study investigated two slopes affected by the 2015 earthquakes in Central Nepal. A combination of TLS, and TDP data supplemented with SfM photogrammetry were employed to monitor the slope behaviour in response to the annual monsoon cycles following the earthquakes. The results demonstrate the potential to apply engineering geomorphology mapping techniques typically used for aerial LiDAR to ground-based LiDAR.

This study underscores the importance of ongoing monitoring to continue to characterize the evolution of earthquake-affected slopes. Future work will include the used of unmanned aerial vehicle (UAV) / helicopter imagery plus high-resolution photogrammetry mapping windows.

7 ACKNOWLEDGEMENTS

We extend our thanks to Brian Collins (USGS) for sharing video footage and imagery of the study area, researchers at Durham for sharing pre-earthquake imagery and field support, our colleagues at the National Society for Earthquake Technology (NSET) for field support and Marc-André Brideau (BGC) for his support and technical guidance.

This work was supported by Mitacs though the Mitacs Accelerate Program. It was made possible thanks to the Natural Sciences and Engineering Research Council of Canada (NSERC) Discovery Grant, Canada Graduate Scholarships-Master's Program, Michael Smith Foreign Study Supplement and support from BGC Engineering.

8 REFERENCES

Adhikari, D.P., and Koshimizu, S. 2005. Debris flow disaster at Larcha, Upper Bhote Koshi Valley, Central Nepal. *The Island Arc*, 14: 410–423.

Agisoft LLC. 2014. PhotoScan Professional Edition.

Barnard, P.L., Owen, L.A., Sharma, M.C., and Finkela, R.C. 2001. Natural and human-induced landsliding in the Garhwal Himalaya of Northern India. *Geomorphology*, 40(1–2): 21–35.

Bommer, J.J., and Rodríguez, C.E. 2002. Earthquake-induced landslides in Central America. Engineering *Geology*, 63(3–4): 189–200.

Collins, B.D. 2015. Video data files to accompany USGS OFR 2015-1142--Assessment of existing and potential landslide hazards resulting from the April 25, 2012 Gorkha, Nepal earthquake sequence. U.S. Geological Survey Data Release.

Collins, B.D., and Jibson, R.W. 2015. Assessment of Existing and Potential Landslide Hazards Resulting from the April 25, 2015 Gorkha, Nepal Earthquake Sequence (ver.1.1, August 2015) *U.S. Geological Survey Open-file Report 2015-1142*. (August): 50.

Cook, K., Andermann, C., Gimbert, F., Hovius, N., and Adhikari, B.R. 2017. Impacts of the 2016 outburst flood on the Bhote Koshi River valley, central Nepal. *In Geophysical Research Abstracts. EGU General Assembly 2017*, Vienna, Austria.

Dhital, M.R. 2015. *Geology of the Nepal Himalaya*. Springer International Publishing, Switzerland.

ESRI. 2017. ArcGIS. ESRI, Redlands, California.

FFmpeg. 2016. ffmpeg. Available from ffmpeg.org.

Girardeau-Montaut, D. 2017. CloudCompare. Available from http://cloudcompare.org/.

Gischig, V.S., Eberhardt, E., Moore, J.R., and Hungr, O. 2015. On the seismic response of deep-seated rock slope instabilities - Insights from numerical modeling. *Engineering Geology*, 193: 1–18. Elsevier B.V.

Gorum, T., Fan, X., Westen, C.J. Van, Qiu, R., Xu, Q., Tang, C., and Wang, G. 2011. Distribution pattern of earthquake-induced landslides triggered by the 12 May 2008 Wenchuan earthquake. *Geomorphology*, 133: 152–167. Elsevier B.V.

Griffiths, J.S., and Whitworth, M. 2012. Engineering geomorphology of landslides. *In* Landslides: Types, Mechanisms and Modeling. *Edited by* J. Clague and D. Stead. Cambridge University Press, New York. pp. 172–186.

ISRM. 1978. Suggested methods for the quantitative description of discontinuities in rock masses. *International Journal of Rock Mechanics and Mining Sciences*, 15: 319–368.

Jibson, R.W. 2011. Methods for assessing the stability of slopes during earthquakes-A retrospective. *Engineering Geology*, 122(1–2): 43–50. Elsevier B.V.

Jibson, R.W., Harp, E.L., and Michael, J.A. 2000. A method for producing digital probabilistic seismic landslide hazard maps. *Engineering Geology*, 58(3–4): 271–289.

Kargel, J.S., Leonard, G.J., Shugar, D.H., Haritashya, U.K., Bevington, A., Fielding, E.J., Fujita, K., Geertsema, M., Miles, E.S., Steiner, J., Anderson, E., Bajracharya, S., Bawden, G.W., Breashears, D.F., Byers, A., Collins, B., Dhital, M.R., Donnellan, A., Evans, T.L., Geai, M.L., Glasscoe, M.T., Green, D., Gurung, D.R., Heijenk, R., Hilborn, A., Hudnut, K., Huyck, C., Immerzeel, W.W., Jiang Liming, Jibson, R., Kääb, A., Khanal, N.R., Kirschbaum, D., Kraaijenbrink, P.D.A., Lamsal, D., Liu Shiyin, Lv Mingyang, McKinney, D., Nahirnick, N.K., Nan Zhuotong, Ojha, S., Olsenholler, J., Painter, T.H., Pleasants, M., Kc, P., Yuan, Q.I., Raup, B.H., Regmi, D., Rounce, D.R., Sakai, A., Shangguan Donghui, Shea, J.M., Shrestha, A.B., Shukla, A., Stumm, D., van der Kooij, M., Voss, K., Wang Xin, Weihs, B., Wolfe, D., Wu Lizong, Yao Xiaojun, Yoder, M.R., and Young, N. 2016. Geomorphic and geologic controls of geohazards induced by Nepal's 2015 Gorkha earthquake. *Science*, 351(6269): 141–151.

Keefer, D.K. 1984. Landslides caused by earthquakes. *Geological Society of America Bulletin*, 95(4): 406–421.

Keefer, D.K. 2000. Statistical analysis of an earthquake-induced landslide distribution - The 1989 Loma Prieta, California event. *Engineering Geology*, 58(3–4): 231–249.

Keefer, D.K. 2002. *Investigating Landslides Caused By Earthquakes – a Historical Review*. 473–510.

Lague, D., Brodu, N., and Leroux, J. 2013. Accurate 3D comparison of complex topography with terrestrial laser scanner: Application to the Rangitikei canyon (N-Z). *ISPRS Journal of Photogrammetry and Remote Sensing*, 82(February 2013): 10–26.

Lin, M., Huang, C., and Kao, T. 2016. Threshold conditions and run-out displacements of the landslides induced by the Chi-Chi earthquake , Taiwan. *In Landslides and Engineered Slopes. Experience, Theory and Practice: Proceedings from the 12th International Symposium on Landslides (Napoli, Italy, 12-19 June 2016). Edited by* C. Aversa, Stefano; Cascini, Leonardo; Picarelly, Luciano; Scavia. CRC Press, Napoli, Italy. pp. 81–90.

Marc, O., Hovius, N., Meunier, P., Uchida, T., and Hayashi, S. 2015. Transient changes of landslide rates after earthquakes. *Geology*, 43(10): 883–886.

Martha, T.R., Roy, P., Mazumdar, R., Govindharaj, K.B., and Kumar, K.V. 2016. Spatial characteristics of landslides triggered by the 2015 Mw 7.8 (Gorkha) and Mw 7.3 (Dolakha) earthquakes in Nepal. Landslides, (April). *Landslides*.

Moore, J.R., Gischig, V., Burjanek, J., Amann, F., and Hunziker, M. 2012. Earthquake-triggered rock slope failures: Damage and site effects. *In Proceedings of the 11th International & 2nd North American Symposium on Landslides*.

National Seismological Centre. 2016. Monthly Epicentre Map.

Oven, K.J. 2009. *Landscape, Livelihoods and Risk: Community Vulnerability to Landslides in Nepal. Durham University*. Available from http://etheses.dur.ac.uk/183/1/Katie_Oven_PhD_thesis_copy_for_submission.pdf?DDD14+.

Owen, L.A., Kamp, U., Khattak, G.A., Harp, E.L., Keefer, D.K., and Bauer, M.A. 2008. Landslides triggered by the 8 October 2005 Kashmir earthquake. *Geomorphology*, 94(1–2): 1–9.

Parker, R.N., Hancox, G.T., Petley, D.N., Massey, C.I., Densmore, A.L., and Rosser, N.J. 2015. Spatial distributions of earthquake-induced landslides and hillslope preconditioning in the northwest South Island, New Zealand. *Earth Surface Dynamics*, 3(4): 501–525.

Petley, D.N., Hearn, G.J., Hart, A., Rosser, N.J., Dunning, S.A., Oven, K., and Mitchell, W.A. 2007. Trends in landslide occurrence in Nepal. *Natural Hazards*, 43(1): 23–44.

Pleiades. 2015. Central Nepal.

RIEGL. 2016. RiSCAN PRO. RIEGL Laser Measurement Systems GmbH, Horn, Austria. Available from riegl.com.

Roback, K., Clark, M.K., West, A.J., Zekkos, D., Li, G., Gallen, S.F., Chamlagain, D., and Godt, J.W. 2016. The size, distribution, and mobility of landslides caused by the 2015 Mw7.8 Gorkha earthquake, Nepal. *Geomorphology*, 301: 121–138.

Robinson, T.R., Rosser, N.J., Densmore, A.L., Williams, J.G., Kincey, M.E., Benjamin, J., and Bell, H.J.A. 2017. Rapid post-earthquake modelling of coseismic landslide intensity and distribution for emergency response decision support. *Natural Hazards and Earth System Sciences,* 17(9): 1521–1540.

Rodríguez, C.E., Bommer, J.J., and Chandler, R.J. 1999. Earthquake-induced landslides: 1980-1997. *Soil Dynamics and Earthquake Engineering*, 18(5): 325–346.

Stead, D., and Eberhardt, E. 2013. Understanding the mechanics of large landslides. *International Conference on Vajont 1963-2013 - Thoughts and analyses after 50 years since the catastrophic landslide,* (6): 85–112.

Tatard, L., and Grasso, J.R. 2013. Controls of earthquake faulting style on near field landslide triggering: The role of coseismic slip. *Journal of Geophysical Research: Solid Earth,* 118(6): 2953–2964.

Tiwari, B., Ajmera, B., and Dhital, S. 2017. Characteristics of moderate- to large-scale landslides triggered by the Mw7.8 2015 Gorkha earthquake and its aftershocks. *Landslides*, 14(4): 1297–1318.

Williams, J.G., Rosser, N.J., Kincey, M.E., Benjamin, J., Oven, K.J., Alexander, L., Milledge, D.G., and Robinson, T.R. 2017. Satellite-based emergency mapping : Landslides triggered by the 2015 Nepal earthquake. *Natural Hazards and Earth System Sciences Discussions* (manuscript under review).

Wolter, A., Gischig, V.S., Eberhardt, E., Stead, D., and Clague, J.J. 2015. Simulation of progressive rock slope failure due to seismically induced damage. *In International Symposium on Rock Slope Stability in Open Pit and Civil Engineering. The South African Institute of Mining and Metallurgy*, Cape Town, South Africa. pp. 529–541.

Yang, W., Qi, W., Wang, M., Zhang, J., and Zhang, Y. 2017. Spatial and temporal analyses of post-seismic landslide changes near the epicentre of the Wenchuan earthquake. *Geomorphology*, 276: 8–15. Elsevier B.V.